Synthesis, Characterization of Novel Modified Reduced Graphene Oxide (RGO) Containing Heterocyclic Compounds

Hussein Ali Fadhil[1*] ✉ and Ali H. Samir[2] ✉

[1,2] Department of Chemistry, College of Education for Pure Science (Ibn Al–Haitham), University of Baghdad, Baghdad, Iraq.

*Corresponding Author.

Abstract

In the present study, nanoderivatives were prepared for graphene sheets that were functionalized with triazoles, starting with the thermal treatment of a mixture of carbon disulfide and hydrazine hydrate, which afforded the thiacarbohydrazide (h5). Treatment of the latter with (salicylic and anthranilic) acid via a fuse heated in solid-state gave (h6) and (h7), respectively. Reaction of L-ascorbic acid with dry acetone in the presence of dry hydrogen chloride afforded the acetone (h1). Treatment of the latter with p-nitrobenzoyl chloride in pyridine yielded the ester (h2), which was dissolved in 65% acetic acid in absolute ethanol and yielded the glycol (h3). The reaction of the glycol with sodium periodate in distilled water at room temperature produced the aldehyde (h4), which was then condensed with compounds (h6, h7) in glacial acetic acid to produce (h8, h9) compounds. In addition, the (II, III, IV) compounds were used to exfoliate graphite (I), which contains graphite rods as both anode and cathode, electrolyte, and distilled water. Sodium bicarbonate is a powerful source for the formation of graphene oxide and graphite oxides with a variable acid (II). Graphene oxide's interaction with hydrazine hydrate yielded (h3). The product of reduced graphene oxide (III) sonification with SoCl2 in dimethylformamide yielded (Acyl-chloride-functionalized Reduced graphene oxide) (IV). Reacting it with compounds (8h, 9h) in dry THF and Et3N produced compounds (h11, h12). The structures of the novel synthesized compounds were confirmed by physical properties and spectral analysis by FTIR spectroscopy, and some of them by 1H,13C-NMR spectra, X-ray diffraction, scanning electron microscope (SEM), and FASEM.

Keywords: Heterocyclic compounds, nanographene oxide, functionalization quinazoline, trizole, vitamin C.

1. Introduction

The notion that Vit-C may play a significant role in cancer prevention which is originally postulated in the 1970s by Cameron and colleagues, who suggested that [1–3] high-dose vitamin C (Vit-C) may increase the survival of cancer patients in their terminal stages. In recent years, the idea that Vit-C could be utilized as a type of anti-cancer treatment has given rise to a number of conflicting claims.

However, recent findings about the pharmacokinetics, physiological properties, and outcomes of preclinical studies indicate that high-dose vitamin C may be useful in the treatment of a variety of tumor forms. Studies have shown that the pharmacological action of vitamin C can attack various processes that cancerous cells use for their growth and development.

Vit-C has several pivotal physiological functions in the body by acting as an electron donor. Not only is it a potent antioxidant, helps to maintain vital tissue structures and functions by protecting key macromolecules such as proteins, fats, and DNA from oxidation.

In a recent study, it was shown that vitamin C plays a pivotal role in controlling gene transcription via its action on transcription factors and epigenetic modifying enzymes [4, 5].

Moreover, vitamin C is frequently supplemented in large amounts to address such shortages; nevertheless, unlike fat-soluble vitamins, toxicity is rare when taken in high concentrations. A wide range of illnesses, such as diabetes (2), atherosclerosis [3], the common cold [4], cataracts [5], glaucoma [6], macular degeneration [7], stroke [8], heart disease [9], COVID-19 [10], and cancer, can be prevented and treated with vitamin C. New findings support the notion that high-dose consumption of Vit-C is associated with a decreased risk of the oral cavity, stomach, esophagus, pancreas, cervix, breast, and rectum cancers [11, 12], and cancers with non-hormonal origins [13].

2. Materials and Methods

All the chemicals and solvents were purchased from A.R. Grade quality obtained from (Aldrich and BDH) was used without further purification. The FTIR Spectra (400–4000) cm^{-1} in KBr disk were recorded on a SHIMADZU FTIR-8400S Fourier transform. The melting point was measured using Stunrt, UK. $^1H, ^{13}C$-NMR were recorded on a Fourier transformation. Burker spectrometer operating at (400MHZ) with (DMSO-d6), XRD, SEM, and FASEM measurements was made at the Department of Chemistry, Esfahan University, Iran.

2.1 Preparation of nanomaterials

2.1.1 Preparation of exfoliated nano-graphite from carbon rods (I)

The electrochemical setup used to exfoliate graphite normally contains the following elements: a graphite rod as both the anode and cathode, an electrolyte (1000 mL distilled water, 10 g sodium bicarbonate) [14], and a power supply of 15 volts for 24 hours, yielding 0.5 g of graphite.

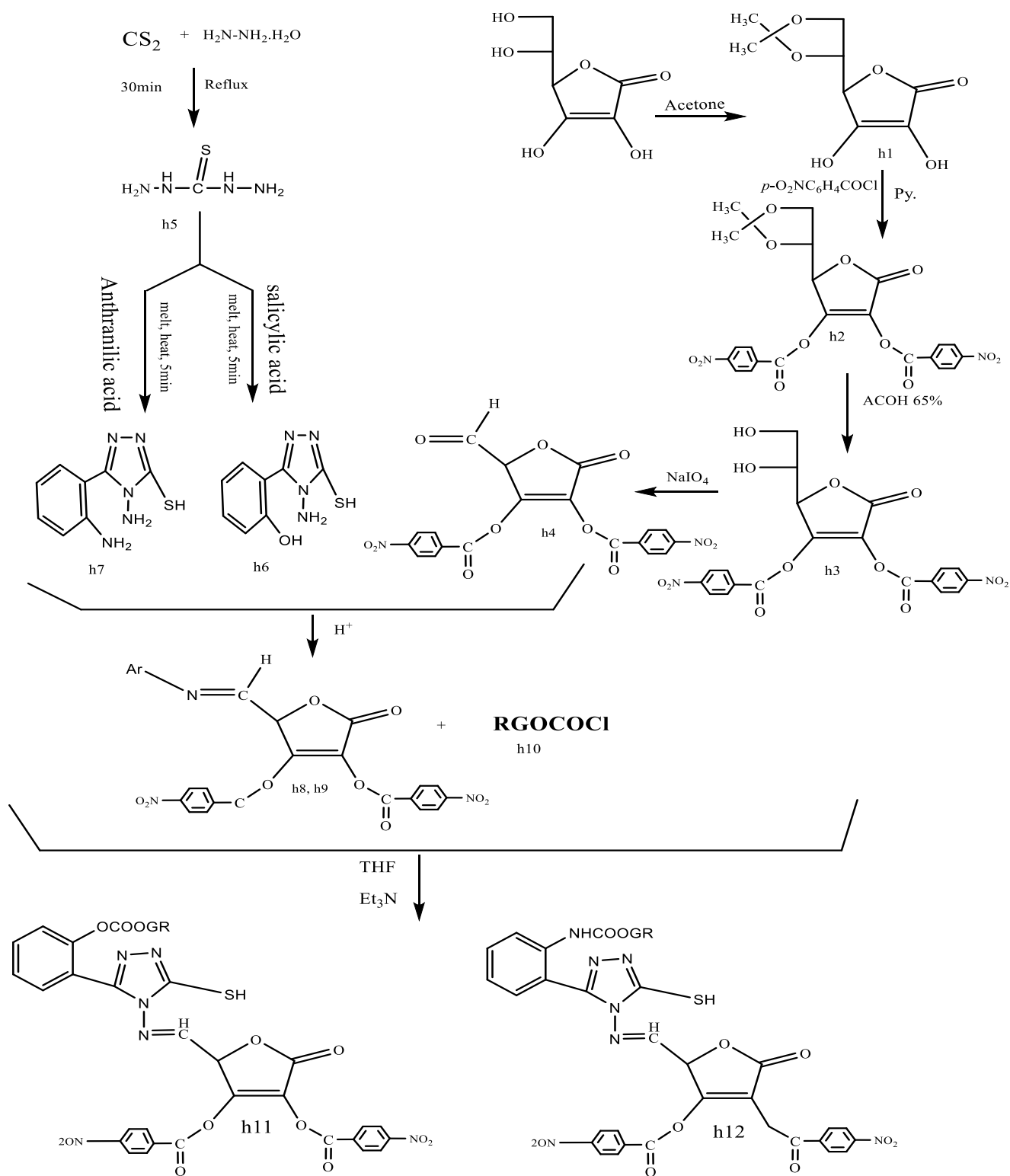### 2.1.2 Preparation of graphene oxide (GO) (II)

Hummer's method was used [15] to oxidize the graphite for the synthesis of GO as follows: Graphite 1g, sodium nitrate (1.5 g), and sulfuric acid (46 mL) were mixed and vigorously stirred at 0°C for 15 minutes in a 500 mL reaction flask immersed in an ice bath. Then, potassium permanganate 6gm was added slowly to the above solution and cooled for 30 minutes. After this, the suspended solution was stirred continuously for 2 hours at 35°C, and water (46 mL) was added slowly to the suspension for 10 minutes and increased the temperature to 98 °C. The solution was left with stirring for 20 minutes. Subsequently, the suspension was diluted with warm water 140 mL and stirred for 10 minutes. After that, the solution was maintained at room temperature and treated with H_2O_2 (15 mL, 30%) to reduce residual permanganate to soluble manganese ions. Finally, the resulting suspension was filtered by the centrifuge, washed with 10% HCL and distilled water [16], and dried in a vacuum oven at 70°C for 24 hours to obtain GO, **Scheme 1**.
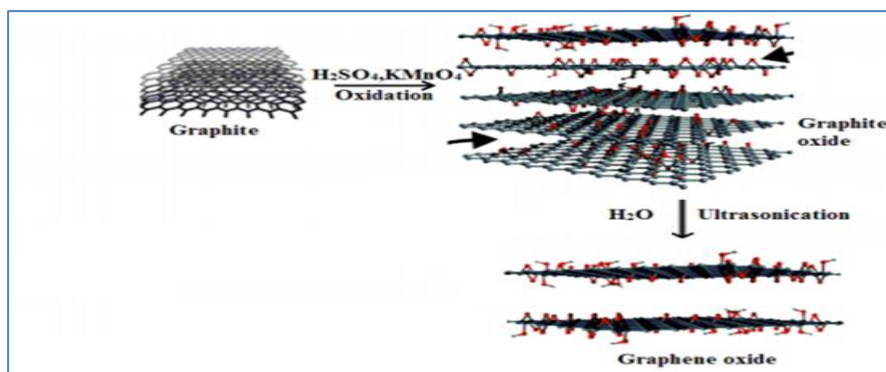
Scheme 1. Oxidation of graphite to graphene oxide.

2.1.3 Preparation of reduced graphene oxide (RGO) by hydrazine (III):

Graphene oxide (100 mg) was dispersed in 1 mL HCl solution. Then, 1 mL of hydrazine monohydrate (80%) was added, and the mixture was heated at 95°C for 2 hours. Then RGO was collected by filtration [17]. The obtained product was washed with water several times to remove the excess hydrazine and dried in a vacuum oven at 100°C for 12 hours, as in **Scheme 2**.

Scheme 2

Scheme 2. Reduce graphene oxide to RGO.

2.1.4 Preparation of acylchloride-functionalized reduced graphene oxide (RGO-COCl)

(IV): About 0.1 g of graphene was well dispersed in 10 mL of dry (DMF) by sonification for 1 hour and then treated with $SOCl_2$ (60 mL, 0.82 mol) at 80°C for 24 hours. The product was separated by the centrifuge, washed with anhydrous THF, and dried, as indicated in **Eq.1** [18].
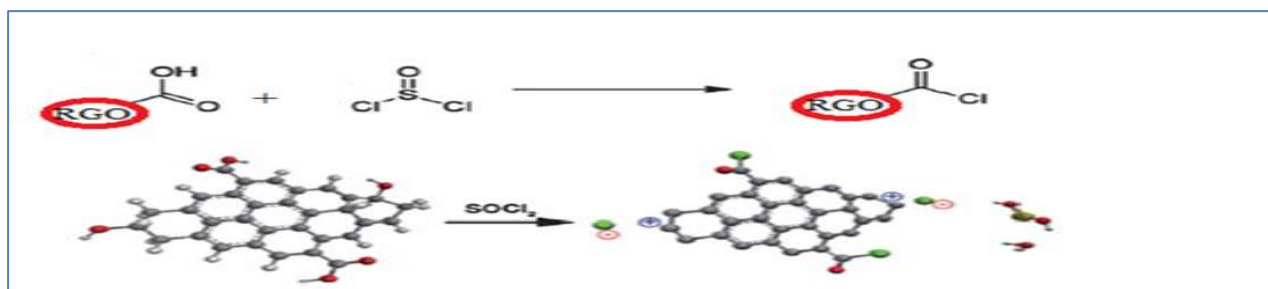
Eq 1. Preparation of acylchloride of RGO.

2.1.5 Synthesis of 5,6-*O*-isopropylidene-L-ascorbic acid (h1)

Dry hydrogen chloride was rapidly bubbled with stirring for 20 minutes into a (250 mL) flask containing (10 g, 57 mmol) of powdered L-ascorbic acid and (100 mL) of dry acetone. After the addition of (80 mL) of n-hexane, stirring, and cooling in ice water, the supernatant was decanted. The residue was washed four times with (154 mL) of the acetone-hexane mixture (4:7) (v/v), with stirring, cooling in ice water, and the removal of the supernatant after each addition [19]. The last residue was dried under reduced pressure to give (h1) (78%) as a white crystalline residue, m.p. (210-212)˚C, (Rf= 0.68; v/v of benzene: methanol, 1:1).

2.1.6 Synthesis of 2,3-*O*-di(*p*-nitrobenzoyl)-5,6-*O*-isopropylidene-L-ascorbic acid (h2)

To a cold solution of (h1) (10 g, 46 mmol) in dry pyridine (50 mL), p-nitrobenzoyl chloride was added (24g, 129 mmol) with stirring. The product mixture was stirred for 2 hours and then kept in a dark place at room temperature for 22 hours.

The mixture was poured into ice water and stirred for 20 minutes. The oil layer was extracted with chloroform (2×150 mL), then washed with water, dilute hydrochloric acid (5%) (2×100 mL), saturated aqueous sodium hydrogen carbonate (100 mL), and water, dried over anhydrous magnesium sulfate. The chloroform vanished [20]. The residue was recrystallized from absolute ethanol to give (h2) (44%) as a brown solid, m.p. (102-104)˚C, (Rf= 0.76; v/v of benzene: methanol 1:1).

2.1.7 Synthesis of 2,3-*O*-di(*p*-nitrobenzoyl) L-ascorbic acid (h3)

Compound (h2) (10 g, 19.45 mmol) was dissolved in a mixture of 65% acetic acid (30 mL) and absolute ethanol (10 mL) and stirred for 48 hrs. at room temperature. The TLC showed that the reaction was complete (benzene:methanol, 6:4). After filtering the mixture, add 40 mL of benzene to the resultant solution, then let it evaporate four times [21]. The residue was recrystallized from absolute ethanol to yield (h3) (74%) as a deep brown solid, m.p. (122–124) ºC, (R$_f$= 0.46; v/v of benzene: methanol, 3:2).

2.1.8 Synthesis of pentulosono-γ-lactone-2,3-enedi(*p*-nitrobenzoate) (h4)

To the stirred solution of sodium periodate (5.6 g , 26 mmol) in distilled water (60 mL) at (0˚C), a solution of h3 (10 g, 21 mmol) in absolute ethanol (60 mL) was added dropwise. After stirring for 15 minutes, ethylene glycol (0.5 mL) was added dropwise, and stirring was continued at room temperature for 1 hour.

The mixture was filtered, and 40 mL of water were added to the filtrate. Next, the product was extracted using three by 50 mL of ethyl acetate, and the extracts were dried using anhydrous magnesium sulfate. Finally, the residue was recrystallized from absolute ethanol, yielding the pure product of (h4) (54%) as a yellow solid, m.p. (194-196)˚C, (Rf= 0.73; v/v of benzene: methanol, 6:4) [22].

2.1.9 Preparation of thiocarbohydrazide (TCH) (h5)

About 5 mL of carbon disulfide was added in a 100 mL round-bottom flask in the ice bath (20 mL), and hydrazinehydrate was added dropwise with stirring. The mixture was refluxed for 30 minutes until a yellow-white precipitate was formed. The yellow-white precipitate was filtered and washed in ethanol and recrystallized from water, and white crystals were formed and dried at 70°C for 4 hrs., m.p. (172-174) °C [23].

2.1.10 Preparation 2-(4-amino-5-mercapto-4H-1,2,4-triazol-3-yl)phenol (h6)

A mixture of salicylic acid (0.01 mol) and thiocarbohydrazide (TCH) (0.02 mol) was placed in an around-bottom flask and heated until melted. The final result after cooling was treated with a sodium bicarbonate solution. After washing the product with water, it was collected by filtration. The solid product was recrystallized from a mixture of dimethylformamide and ethanol, as indicated in Scheme (3), m.p. (236-238) °C [24].

2.1.11 Preparation of 4-amino-5-(2-aminophenyl)-4H-1,2,4-triazole-3-thiol (h7)

Placed in an around-bottom flask, a combination of 2-aminobenzoic acid (0.01 mol) and thiocarbohydrazide (TCH) (0.02 mol) was heated until melted. After cooling, the product was treated with a sodium bicarbonate solution. Then, water was used to rinse and filter the product. A combination of dimethylformamide and ethanol was used to recrystallize the solid product, m.p. (236-238) [25].

2.1.12 Synthesis of Schiff bases (h8) and (h9)

A mixture of compounds (h6) and (h7) (0.5 mmol) with an aldehyde (h4) (0.2 g, 0.5 mmol), absolute ethanol (10 mL), and 3 drops of glacial acetic acid was refluxed for 48 hours, the solvent was evaporated, and the residue was recrystallized from absolute ethanol to yield the Schiff bases (h8) and (h9) [26]. The nomenclature and physical properties of synthesized Schiff bases are listed in **Table 3**.

3. Results

As a result of the remarkable structural and chemical properties of graphene and GO, their application for drug delivery has increased in the past several years. Previous studies clearly indicate that significant and exciting progress has been made in this field and demonstrate the great potential of this emerging biomaterial for biomedical applications. Although preliminary preclinical studies are encouraging, the field is still far from clinical applications, which require addressing some remaining challenges. Graphene and GO obviously display many advantages compared with other drug-delivering systems, with the ability to provide high drug-loading capacity for many different drugs and therapeutic molecules using straightforward preparation procedures. Both covalent and non-covalent surface modifications have been successfully used to impart specific biological activity to graphene and GO, as well as to improve biocompatibility and colloidal stability. Their flexibility and capability to design complex multifunctional drug delivery systems for combined therapies is a new direction hardly possible with other nanomaterials. To this end, control of the size and number of single layers of graphene separated from bulk graphite is still a challenging issue that needs to be solved in order to develop these nano-carriers with reproducible dimensions and properties.

One of the most critical questions about these materials is a profound understanding of graphene's interaction with living cells (tissues and organs), especially the cellular uptake mechanism. This knowledge will undoubtedly facilitate the future development of graphene-based nano-carriers,

especially for anticancer therapy, where these materials showed considerable potential. The most critical issue for the biomedical application of these materials is their biocompatibility and toxicity, which is a primary concern. The current literature has revealed the majority of present studies indicate that graphene is biocompatible and a low-toxic material. However, caution must be taken with conflicting and unclear results obtained by different research groups. However, an agreement has been gradually reached that the functionalization of pristine graphene and GO significantly improves their biocompatibility, and this step is essential for designing stable and safe drug delivery nano-carriers.

4. Discussion

4.1 Preparation and characterization 5,6-*O*-isopropylidene-L-ascorbic acid (h1)

Compound (h1) was prepared from the reaction of L-ascorbic acid with acetone in acidic media using the Salomon method [27]. The FTIR spectrum of compound (h1) in **Figure 1** showed the following bands: stretching bands at (3244) cm^{-1} for (O-H) vinylic, stretching bands at (2993, 2910) cm^{-1} for (C-H) aliphatic, acetal linkage, stretching band at (1751) cm^{-1} for (C=O) lactone ring, stretching band at (1660) cm^{-1} for (C=C), bending bands symmetrical and asymmetrical at (1379, 1435) cm^{-1} for (C-H) aliphatic, stretching bands at (1140–900) cm^{-1} for (C-O), and bending band at (768) cm^{-1} for (O-H) (O.O.P.).
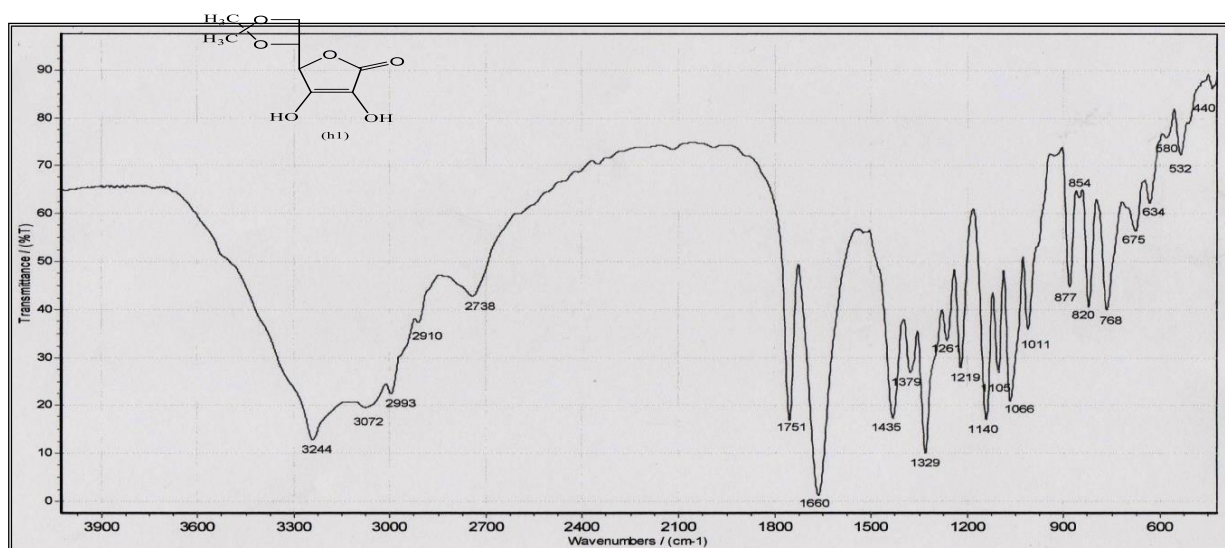

Figure 1. The FTIR spectrum of compound (h1).

4.2 Preparation and characterization 2,3 -*O*-di(*p*-nitrobenzoyl)-5,6-*O*-isopropylidene-L-ascorbic acid (h2)

Compound (h1) reacts with an excess of *p*-nitrobenzoyl chloride in dry pyridine to give compound (h2). The FTIR spectrum of compound (h2) in **Figure 2** showed stretching bands at (1693) cm^{-1} for (C=O) of the ester and disappearance of the stretching bands for (O-H) of compound (h1), stretching bands at (3078) cm^{-1} for (C-H) aromatic, stretching bands at (2987, 2943) cm^{-1} for (C-H) aliphatic, acetal linkage, stretching band at (1745) cm^{-1} for (C=O) lactone ring, stretching bands at (1606) cm^{-1} and (1421) cm^{-1} for (C=C) aliphatic and aromatic, bands at

(1346, 1531) cm^{-1} for symmetrical and asymmetrical stretching vibration of (NO$_2$), stretching bands at (1263–1105) cm^{-1} for (C-O) and (900–600) cm^{-1} for (C-H) aromatic bending (O.O.P.).
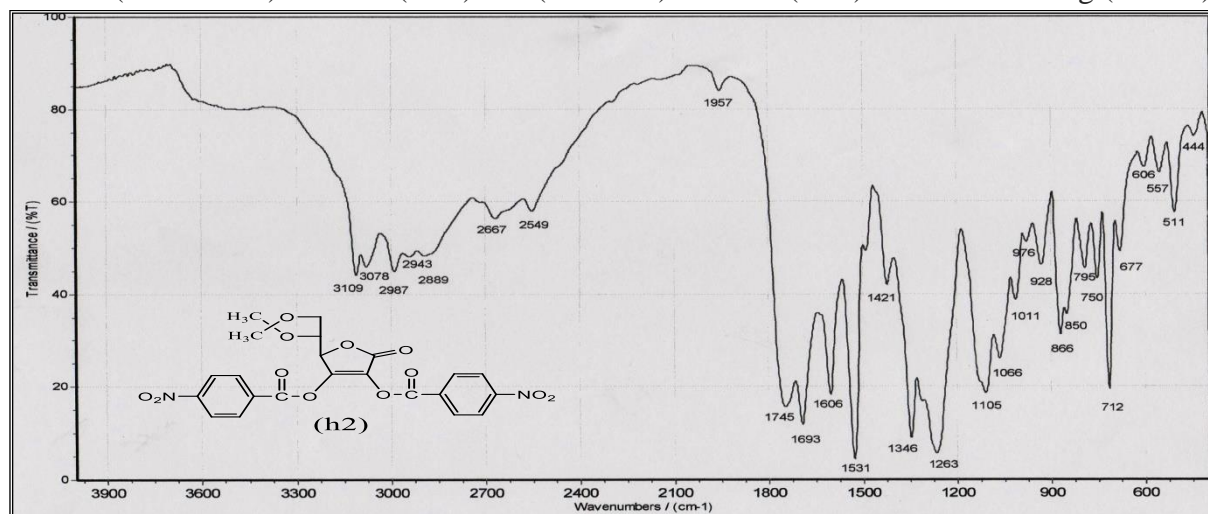

Figure 2. The FTIR spectrum of compound (h2).

4.3 Preparation and characterization2,3-*O*-di(*p*-nitrobenzoyl)-L-ascorbic acid (h3)

The isopropylidene ring may be hydrolyzed in acidic media easily, as mentioned in the introduction; we used (65%) acetic acid to hydrolyze the acetal's ring. The FTIR spectrum of compound (h3) in **Figure 3** showed a stretching broad band at (3413) cm^{-1} for (O-H), a stretching band at (3078) cm^{-1} for (C-H) aromatic, a stretching band at (2985) cm^{-1} for (C-H) aliphatic, a stretching band at (1720) cm^{-1} for (C=O) of the ester, a stretching band at (1603) cm^{-1} for (C=C) aromatic, bands at (1358, 1520) cm^{-1} for symmetrical and asymmetrical stretching vibration of (NO$_2$), a stretching band at (1275-1105) cm^{-1} for (C-O), and a stretching band at (900-600) cm^{-1} for (C-H) aromatic bending (O.O.P.)
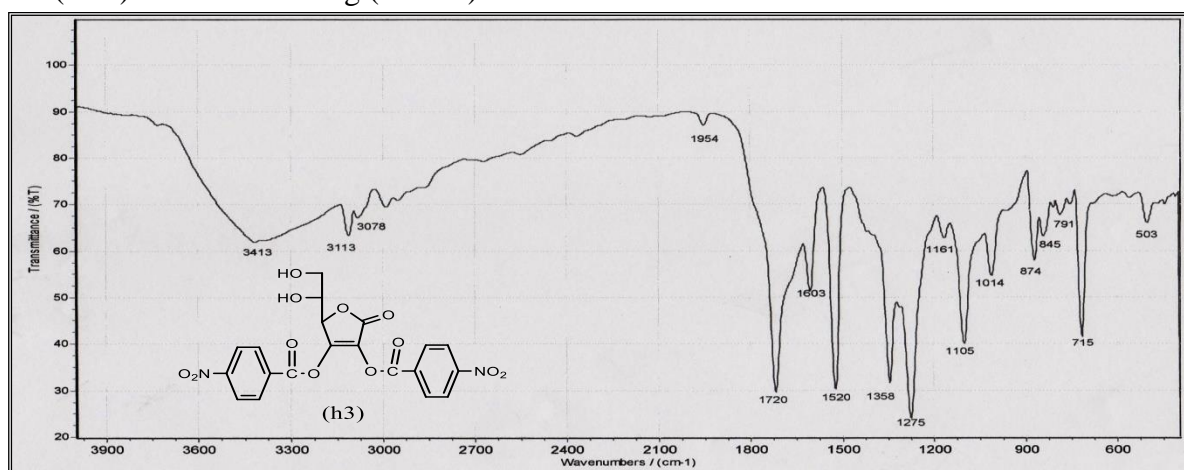

Figure 3. The FTIR spectrum of compound (h3).

4.4 Preparation and characterization of pentulosono-γ-lactone-2,3-enedi(*p*-nitrobenzoate) (h4)

Glycols (compounds that contain two vicinal hydroxyl groups) are oxidized by periodate, which cleaves the carbon-carbon (bearing OH groups) bond and forms two compounds containing carbonyl groups. The compound (h4) was characterized by FTIR, ^{1}H-NMR and ^{13}C-

NMR. The FTIR spectrum of compound (h4) in **Figure 4** showed the following bands: stretching bands at (2841, 2740) cm^{-1} for (C-H) aldehydic, stretching bands at (3068, 2993) cm^{-1} for (C-H) aromatic, aliphatic, stretching band at (1697) cm^{-1} for (C=O) aldehydic, bands at (1356 and 1535) cm^{-1} for symmetrical and asymmetrical stretching vibration of (NO$_2$), and bands at (900–600) cm^{-1} for aromatic bending (O.O.P).
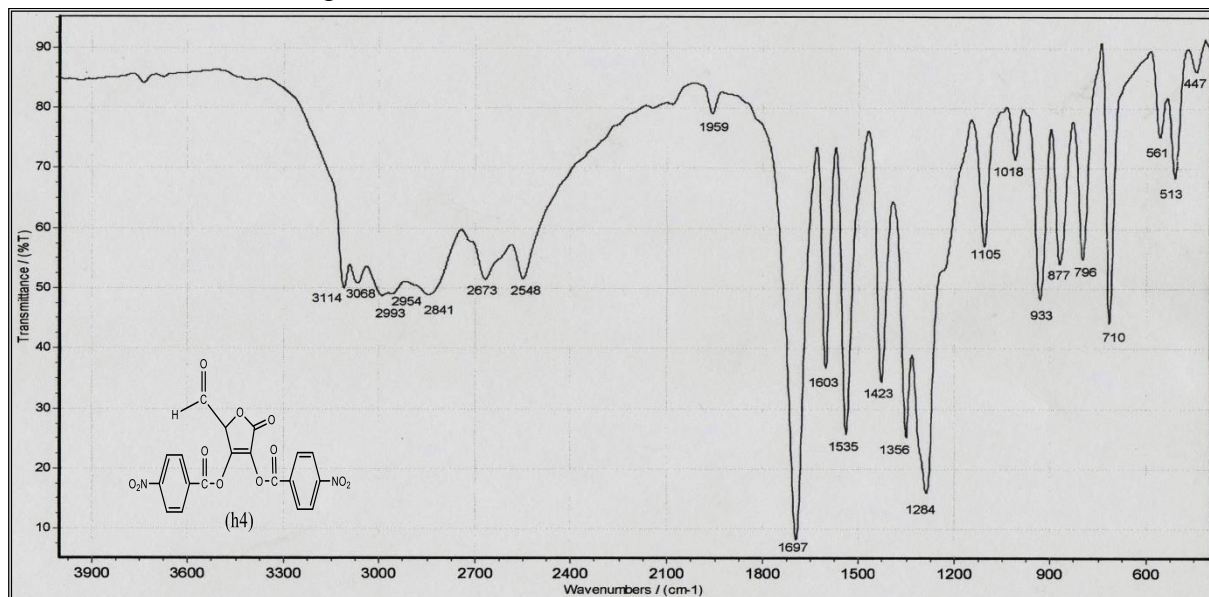

Figure 4. The FTIR spectrum of compound (h4).

The ^{1}H-NMR spectrum of compound (h4) for DMSO-d$_6$ in **Figure 5** showed the following signals: singlet peak at δ(2.5) ppm for DMSO, singlet peak at δ(3.92) ppm for (^{1}H, lactone ring H-4), doublet peaks at δ(8.15-8.34) ppm for aromatic protons, singlet peak at δ(9.11) ppm for (1H, CHO).
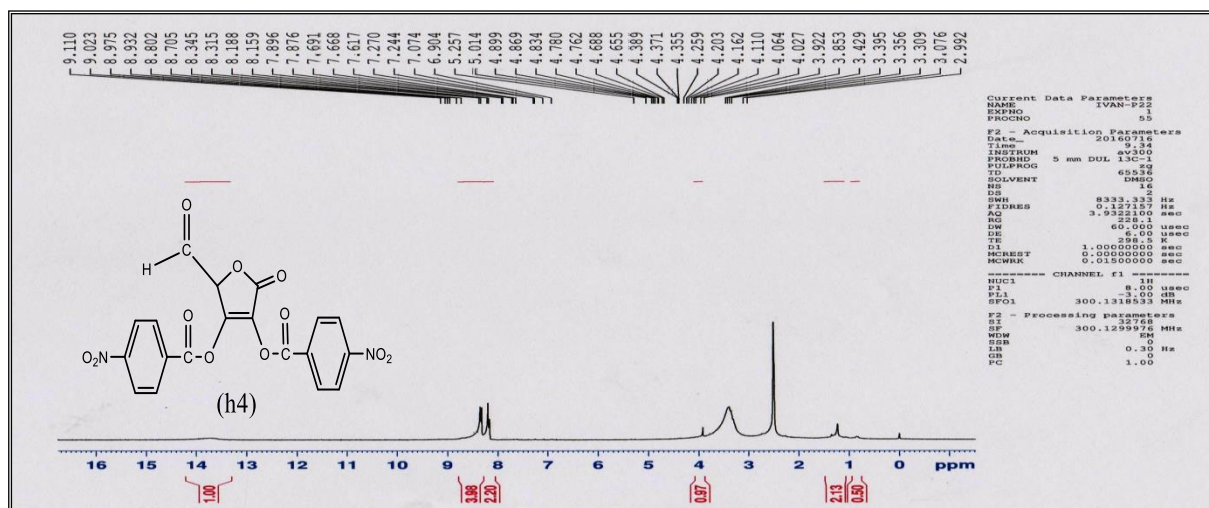

Figure 5. 1H-NMR spectrum of compound (h4)

The ^{13}C-NMR spectrum of compound (h4) in DMSO-d$_6$ in **Figure 6** showed the following signals: signal at δ(38.63-40.29) ppm for DMSO, signal at δ(47.99) ppm for (C-4), signal at

δ(105.85) ppm for (C-2), signals at δ(123.58-136.32) ppm for aromatic carbons, signal at δ(149.99) ppm for (C-3), signal at δ(167.48) ppm for (C=O) ester, signal at δ(178.58) ppm for (C=O) lactone ring and (C=O) aldehydic [28].
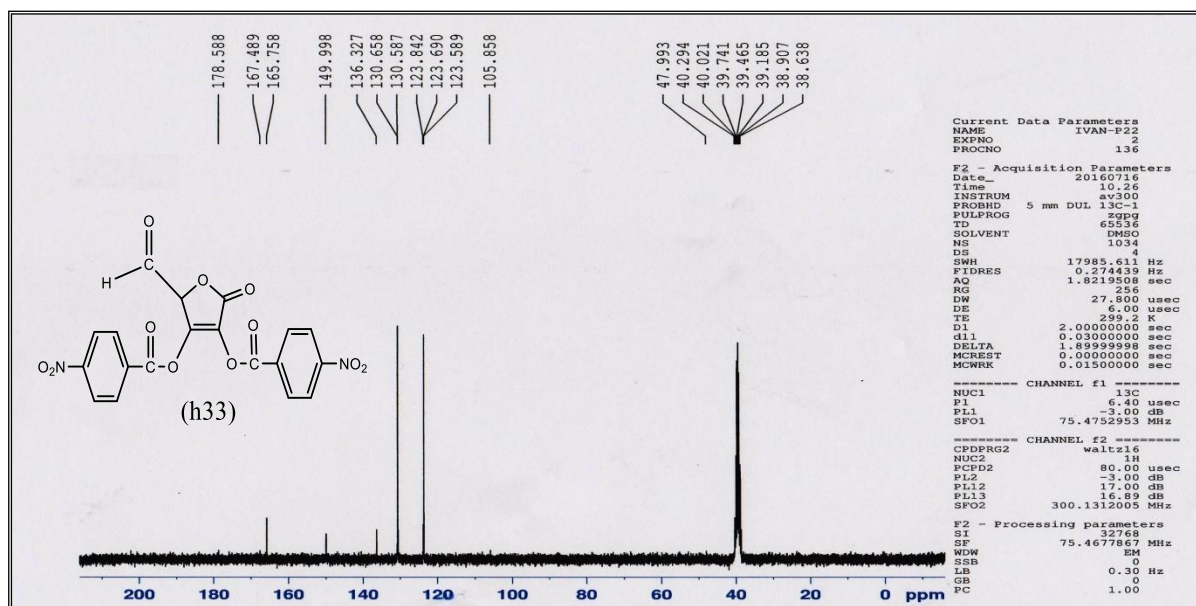

Figure 6. 13C-NMR spectrum of compound (h4)

4.5 Compound (h5): Thiocarbohydrazide (TCH)

However, the most popular method of producing TCH is turning carbon disulfide into hydrazine. Carbon disulfide reacts with hydrazine to produce hydrazinium dithiocarbazinate (HDTC), a water-soluble salt formed in nearly quantitative yield at relatively low temperatures [29]. The FT-IR spectrum data of compound (I) showed peaks at 3304, 3269, 3165 cm^{-1} corsspondes to N-H and NH$_2$ stretching vibrations, respectively.

The NH$_2$ bending and wagging vibrations contributed to the two peaks at 1637 and 1139 cm^{-1}, respectively. The characteristic peaks at 1531 and 1490 cm^{-1} correspond to the coupled modes of N-H wagging and C-N stretching vibrations. The C=S stretching contributes to two peaks at 1284 cm-1 and 927 cm^{-1}. These peaks also contain contributions from other vibrations, such as C-N stretching and C-N-N bending vibrations.

4.6 Compound (h6): 4-amino-5-(2-aminophenyl)-4H-1,2,4-triazole-3-thiol

The compound (II) showed stretching vibration of v (NH$_2$) in (3422, 3367) cm^{-1} while the v (O-H) was inserted with v (NH). The peak in 1651 is assigned to the v(C=N). The C=S stretching contributes to the peak at 1161 cm^{-1}, and the peak at 1086 cm^{-1} corresponds to v(N-N) [30]

4.7 Compound (h7): 4-amino-5-(2-aminophenyl)-4H-1,2,4-triazole-3-thiol

The FT-IR spectrum data of compound [II] showed stretching vibrations of v (NH$_2$) aliphatic in (3522, 3367.71) cm^{-1} and v (NH$_2$) aromatic in (3400, 3263.1) while v (NH) was interested. The peak in (1666.5) is assigned to the v(C=N). The C=S stretching contributes to the peak at 1149.58 cm^{-1},also the peak at 10725 cm^{-1} corresponds to v(N-N) [30].

4.8 Preparation and characterization of Schiff bases (h8) and (h9):

The novel Schiff bases were synthesized by refluxing equimolar aldehyde (h4) with compounds (h6) or (h7) in absolute ethanol with some drops of glacial acetic acid (GAA). These Schiff bases (h8) and (h9) were identified by their melting points, FTIR, ^{1}H-NMR and ^{13}C-NMR spectroscopy. The FTIR spectra of Schiff bases (h8, h9) showed the disappearance of absorption bands of (NH$_2$) and (C=O) groups of the starting materials, together with the appearance of new absorption stretching bands at (1658) cm^{-1} and (1681) cm^{-1} which are assigned to azomethine group (C=N) stretching.
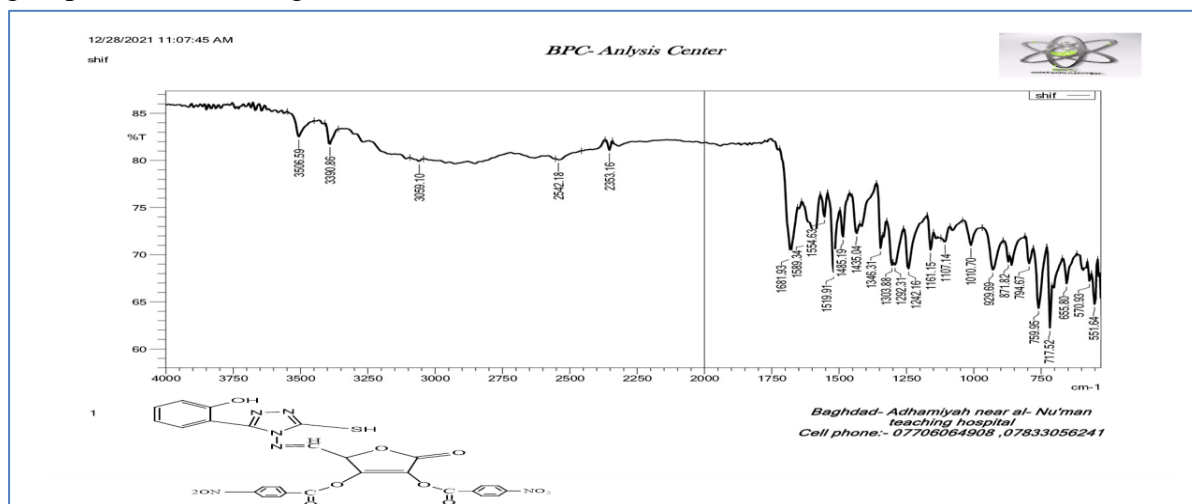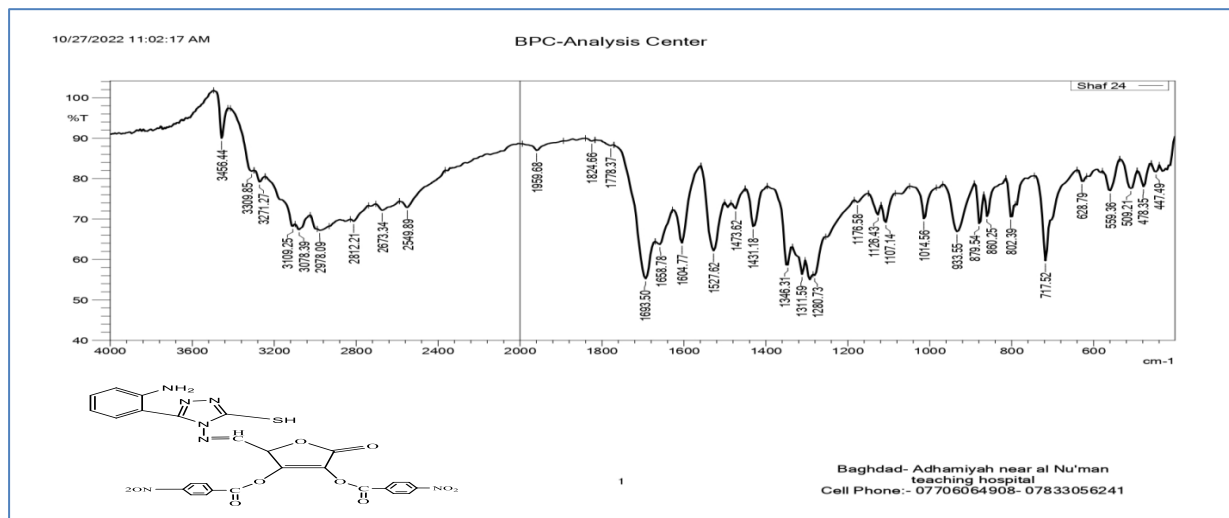

Figure 7. The FTIR spectrum of compound (h8).

Figure 8. FTIR spectrum of compound (h9).

The ^{1}H-NMR spectrum (in DMSO-d6) as a solvent of compound (h8) in **Figure 9** showed the following signals: singlet peak at δ(6.05) ppm for (NH), a singlet signal at (8.53) ppm for (CH) of imine group, a singlet signal at δ (12.57) ppm for (OH) of imine, singlet signal at δ(13.68) ppm for (SH), the signals appeared at δ(6.85-8.47) ppm for aromatic protons.

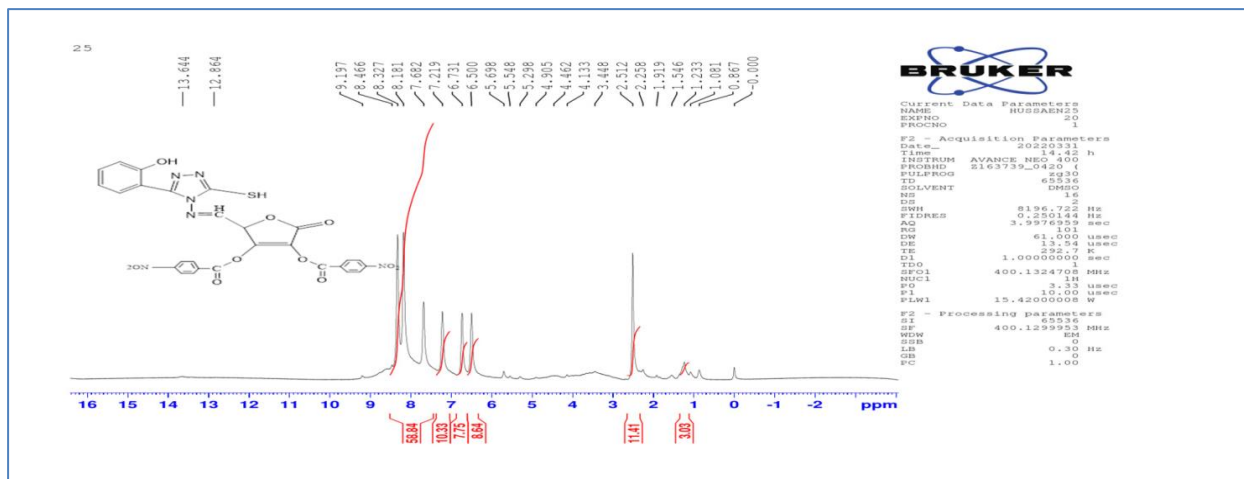**Figure 9.** The ^{1}H-NMR spectrum of compound (h8).

The ^{1}H-NMR spectrum (in DMSO-d6) as a solvent of compound (h9) in **Figure 10** showed the following signals: singlet peak at δ(5.29) ppm for (NH$_2$), a singlet signal at (6.5) ppm for (NH), a singlet signal at δ (9.19) ppm for (-CH=N-) of imine, a singlet signal at δ(13.64) ppm for (SH), the signals appeared at δ(6.73-8.32) ppm for aromatic protons.
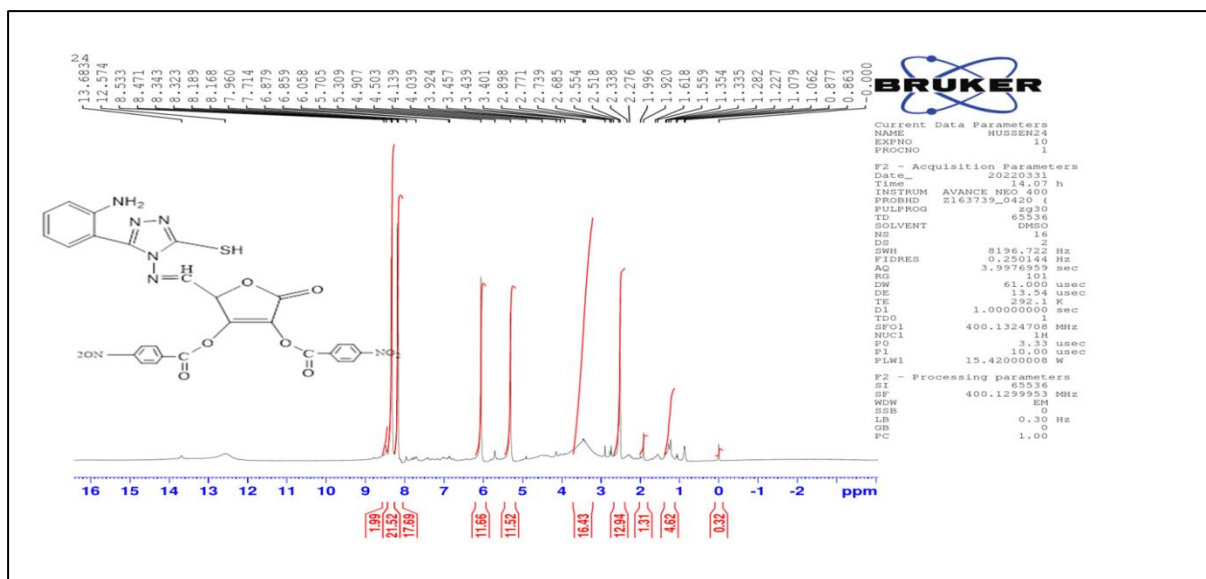

Figure 10. The ^{1}H-NMR spectrum of compound (h9).

4.9 Preparation and characterization of graphene- triazol Schiff base (h11, h12)

The compound (h11) in **Figure 11** and **Table 1** illustrates the presence of a large peak at (3379) cm^{-1}. This peak is related to the stretching of the ν (OH) group for RGO and the appearance of an absorption band at (1710) cm^{-1} due to the carbonyl group of the ester. The imine group appeared at ν (1627) cm^{-1}
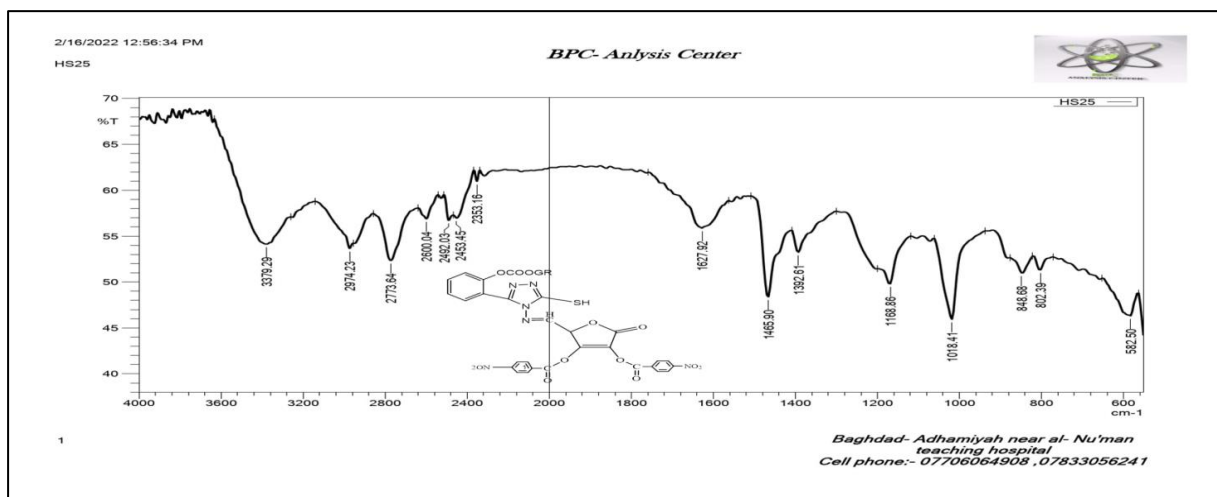
Figure 11. The FT-IR spectrum of (h11) compound.

The compound (h12) in **Figure 12** and **Table 1** illustrates the presence of a large peak at (3387) cm^{-1}.This peak is related to the stretching of the v (OH) group for RGO and the appearance of an absorption band at (1690) cm^{-1} due to the carbonyl group of the ester. The imine group appeared at v(1720) cm^{-1}
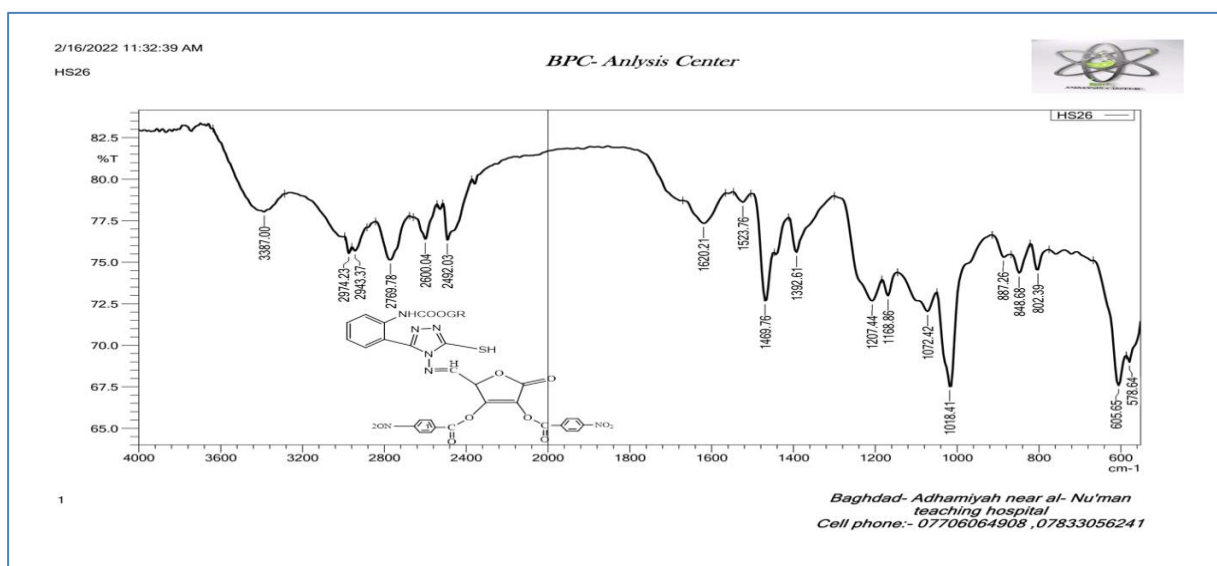

Figure 12. The FT-IR spectrum of (h12) compound.

5. Conclusion

Therefore, more toxicity studies using in vivo animal models are required in the future to prove the biocompatibility of graphene and GO. Finally, the recent advances in graphene-based nano-carriers for drug delivery applications is a significant development in nanomedicine. This opens exciting opportunities for the future and broad use of nanomaterials in actual clinical conditions.

Conflict of Interest

The authors declare that they have no conflicts of interest.

Funding

There is no funding for the article.

References

1. Zhang, J.; Rao, X.; Li, Y.; Zhu, Y.; Liu, F.; Guo, G.; Luo, G.; Meng, Z.; De Backer, D.; Xiang, H.; Peng, Z. Pilot Trial of High-dose Vitamin C in Critically ll COVID-19 Patients. *Annals of Intensive Care*, **2021**, *11*, 1-12. DOI: https://doi.org/10.1186/s13613-020-00792-3

2. Cameron, E.; Campbell, A. The Orthomolecular Treatment of Cancer. II. Clinical Trial of High-Dose Ascorbic Acid Supplements in Advanced Human Cancer. *Chemico-Biological Interactions* **1974**, *9(4)*, 285–315. https://doi.org/10.1016/0009-2797(74)90019-2

3. Cameron, E.; Pauling, L. Supplemental Ascorbate in the Supportive Treatment of Cancer: Prolongation of survival times in terminal human cancer. *Proc. Natl. Acad. Sci. USA* **1976**, *73*, 3685–3689. https://doi.org/10.1073/pnas.73.10.368

4. Carr, A.C.; McCall, C. The role of vitamin C in the treatment of pain: New insights. *Journal of Translational Medicine.* **2017**, *15(1)*, 77. doi: https://doi.org/10.1111/Jan.1314.

5. Ting, H.H.; Timimi, F.K.; Boles, K.S.; Creager, S.J.; Ganz, P.; Creager, M.A. Vitamin C improves endothelium-dependent vasodilation in patients with non-insulin-dependent diabetes mellitus. *J. Clin. Investig.* **1996**, *97*, 22–28. https://doi.org/10.1172/JCI118394.

6. Valero, M.P.; Fletcher, A.E.; De Stavola, B.L.; Vioque, J.; Alepuz, V.C. Vitamin C is associated with reduced risk of cataract in aMediterranean population. *J. Nutr.* **2002**, *132*, 1299–1306. https://doi.org/10.1093/jn/132.6.1299

7. Ramdas, W.D.; Schouten, J.; Webers, C.A.B. The Effect of Vitamins on Glaucoma: A Systematic Review and Meta-Analysis.Nutrients 2018, 10, 359. https://doi.org/10.3390/nu10030359

8. Seddon, J.M.; Ajani, U.A.; Sperduto, R.D.; Hiller, R.; Blair, N.; Burton, T.C.; Farber, M.D.; Gragoudas, E.S.; Haller, J.; Miller,D.T.; et al. Dietary carotenoids, vitamins A, C, and E, and advanced age-related macular degeneration. Eye Disease Case-Control Study Group. *Jama* **1994**, *272*, 1413–1420. doi: https://doi.org/10.1001/jama.1994.03520180037032

9. Chen, G.C.; Lu, D.B.; Pang, Z.; Liu, Q.F. Vitamin C intake, circulating vitamin C and risk of stroke: A meta-analysis of prospective studies. *J. Am. Heart Assoc.* **2013**, *2*, e000329. https://doi.org/10.1161/JAHA.113.000329

10. Losonczy, K.G.; Harris, T.B.; Havlik, R.J. Vitamin E and vitamin C supplement use and risk of all-cause and coronary heart disease mortality in older persons: The Established Populations for Epidemiologic Studies of the Elderly. *Am. J. Clin. Nutr.* **1996**, *64*, 190–196. https://doi.org/10.1093/ajcn/64.2.190

11. Moertel, C.G.; Fleming, T.R.; Creagan, E.T.; Rubin, J.; O'Connell, M.J.; Ames, M.M. High-dose vitamin C versus placebo in the treatment of patients with advanced cancer who have had no prior chemotherapy. A randomized double-blind comparison. *N.Engl. J. Med.* **1985**, *312*, 137–141. DOI: https://doi.org/10.1056/NEJM198501173120301

12. Block, G. Vitamin C and cancer prevention: The epidemiologic evidence. *Am. J. Clin. Nutr.* **1991**, 53 (Suppl. 1), 270s–282s. DOI: https://doi.org/10.1056/NEJM198501173120301

13. Block, G. Epidemiologic evidence regarding vitamin C and cancer. *Am. J. Clin. Nutr.* **1991**, 54 (Suppl. 6), 1310s–1314s. https://doi.org/10.1093/ajcn/54.6.1310s

14. Biranje, P. M.; Patwardhan, A. W.; Joshi, J. B.; Dasgupta, K. (**2022**). Exfoliated graphene and its derivatives from liquid phase and their role in performance enhancement of epoxy matrix composite.

Composites Part A: Applied Science and Manufacturing, 106886. https://doi.org/10.1016/j.compositesa.2022.106886

15. Kumar P.; Subrahmanyam, K.; Rao, C. Graphene produced by radiation-induced reduction of graphene oxide, *International Journal of Nanoscience*, **2011,***10*,559-566, https://doi.org/10.1142/S0219581X11008824.

16. Shahriary, L.; Athawale, A. A. Graphene oxide synthesized by using modified hummers approach, Int *J Renew Energy Environ Eng*, **2014,** *2*, 58-63,.

17. Chauhan, D. S. ; Ansari, K. ; Sorour, A.; Quraishi, M.; Lgaz, H.; Salghi, R. Thiosemicarbazide andthiocarbohydrazide functionalized chitosan as ecofriendly corrosion inhibitors for carbon steel inhydrochloric acid solution," International journal of biological macromolecules **2018,** *107*, 1747-1757, https://doi.org/10.1016/j.ijbiomac.2017.10.050

18. Namvari, M.;Namazi, H. Synthesis of magnetic citric-acid-functionalized graphene oxide and its application in the removal of methylene blue from contaminated water. *Polymer international*, **2014,***63*(*10*), 1881-1888. https://doi.org/10.1002/pi.4769

19. Salomon, L. L. *Experientia*, **1963,***19*(*12*), 619 .

20. Fadhil, H. A.; Samir, A. H.; Rumez, R. M. Synthesis and Characterization of some New Oxazepine Compounds Derived from D-Erythroascorbic Acid. *Iraqi National Journal of Chemistry*, **2016,***16*(*4*) http://www.ripublication.com

21. Salman, A. O.; AlAbassi, H.; Mahod, W.. Demographic and Clinico-Pathological Characteristics of Some Iraqi Female Patients Newly Diagnosed with Breast Cancer. *Annals of the Romanian Society for Cell Biology*, **2021,***25*(*6*), 8264-8278. 8264 http://annalsofrscb.ro

22. Suhail, N. et al. Effect of vitamins C and E on antioxidant status of breast-cancer patients undergoing chemotherapy. *Journal of clinical pharmacy and therapeutics* **2012,** *37*(*1*), 22-26 https://doi.org/10.1111/j.1365-2710.2010.01237.x

23. Chauhan, D. S.; Ansari, K. R.; Sorour, A. A.; Quraishi, M. A.;Lgaz, H.;Salghi, R. Thiosemicarbazide and thiocarbohydrazide functionalized chitosan as ecofriendly corrosion inhibitors for carbon steel in hydrochloric acid solution. International journal of biological macromolecules **2018,***107,* 1747-175.https://doi.org/10.1016/j.ijbiomac.2017.10.050.

24. Moorthy, N. H. N.; Vittal, U. B.; Karthikeyan, C.; Thangapandian, V.; Venkadachallam, A.; Trivedi, P. Synthesis, antifungal evaluation and in silico study of novel Schiff bases derived from 4-amino-5 (3, 5-dimethoxy-phenyl)-4H-1, 2, 4-triazol-3-thiol, *Arabian Journal of Chemistry* **2017,***10*, S3239-S3244.DOI: https://doi.org/10.1016/j.arabjc.2013.12.021.

25. Vogel, 1989, Vogel's Textbook of Practical Organic Chemistry, 5th Ed., John Wiley and Sons, Inc., New York, 1219.

26. Al-Bayati, A. T., , July. Measurement of uranium concentration in the water samples collected from the areas surrounding in Al-Tuwaitha nuclear site using the CR-39 detector. In Journal of Physics: *Conference Series* **2019** ,*1234*,(*1*), 012007. IOP Publishing doi: https://doi.org/10.1088/1742-6596/1234/1/012007.

27. Carey, F. A. Organic Chemistry, 6th Ed., the McGraw-Hill Companies, Inc., New York, 767 (**2006**).

28. Zhou, J.; Wu, D.; Guo, D. Optimization of the production of thiocarbohydrazide using the Taguchi method. Journal of Chemical Technology & Biotechnology **2010**, *85*(*10*), 1402-1406. https://doi.org/10.1002/jctb.2446